

*Electronic Supplementary Information (ESI)*

**Probing Photophysical Properties of Isomeric N-heterocyclic Carbene Ir(III) Complexes  
and their Applications to Deep Blue Phosphorescent Organic Light-Emitting Diodes**

Yang-Jin Cho,<sup>a</sup> So-Yoen Kim,<sup>a</sup> Jin-Hyoung Kim,<sup>a</sup> Jiewon Lee,<sup>b</sup> Dae Won Cho,<sup>a</sup> Seungjun Yi,<sup>a</sup> Won-Sik Han,<sup>b</sup> Ho-Jin Son,<sup>a</sup> and Sang Ook Kang<sup>a</sup>

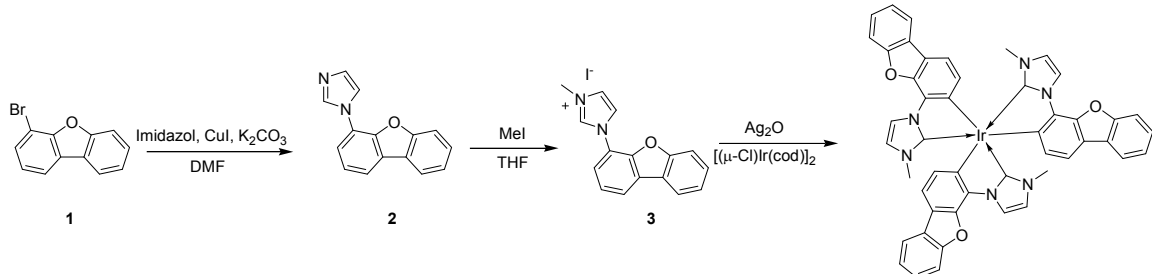
<sup>a</sup>Department of Advanced Materials Chemistry, Korea University, Sejong 30019, South Korea,

<sup>b</sup>Department of Chemistry, Seoul Women's University, Seoul 01797, South Korea.

**Synthetic details**

<b>Fig. S1</b>	<sup>1</sup> H-NMR spectra of 1-(dibenzo[ <i>b,d</i> ]furan-4-yl)-3-methyl-1 <i>H</i> -imidazol-3-ium iodide.	S2
<b>Fig. S2</b>	<sup>1</sup> H-NMR spectra of <b>f-Ir-(dbfmi)<sub>3</sub></b> before (top) and after (down) vapor deposition.	S3
<b>Fig. S3</b>	<sup>1</sup> H-NMR spectra of <b>m-Ir-(dbfmi)<sub>3</sub></b> before (top) and after (down) vapor deposition.	S4
<b>Fig. S4</b>	ORTEP drawing of <b>m-Ir-(dbfmi)<sub>3</sub></b> .	S5
<b>Table S1.</b>	Crystal data and structure refinement for <b>m-Ir-(dbfmi)<sub>3</sub></b> .	S6
<b>Table S2.</b>	Bond lengths [Å] for <b>m-Ir-(dbfmi)<sub>3</sub></b> .	S7
<b>Table S3.</b>	Angles [°] for <b>m-Ir-(dbfmi)<sub>3</sub></b> .	S8
<b>Fig. S5</b>	Contour plots of selected orbitals calculated for <b>f-Ir-(dbfmi)<sub>3</sub></b> and <b>m-Ir-(dbfmi)<sub>3</sub></b> in the singlet ground state geometry.	S9
<b>Fig. S6</b>	The electroluminescent (EL) spectra of devices <b>I</b> and <b>II</b> .	S11
<b>Fig. S7</b>	Experimental absorption spectra and calculated singlet transition for <b>f-Ir-(dbfmi)<sub>3</sub></b> and <b>m-Ir-(dbfmi)<sub>3</sub></b> .	S12
<b>Table S4.</b>	Energy levels of the lower lying transitions of complex <b>f-Ir-(dbfmi)<sub>3</sub></b> and <b>m-Ir-(dbfmi)<sub>3</sub></b> , calculated from the TD-DFT approach.	S13
<b>Fig. S8</b>	Emission decay profiles for <b>f-Ir-(dbfmi)<sub>3</sub></b> and <b>m-Ir-(dbfmi)<sub>3</sub></b> in doped films ( <b>f-Ir-(dbfmi)<sub>3</sub></b> or <b>m-Ir-(dbfmi)<sub>3</sub></b> (5%):TSPO1 (100 nm)).	S14
<b>Fig. S9</b>	Emission spectra for <b>f-Ir-(dbfmi)<sub>3</sub></b> and <b>m-Ir-(dbfmi)<sub>3</sub></b> in doped films ( <b>f-Ir-(dbfmi)<sub>3</sub></b> or <b>m-Ir-(dbfmi)<sub>3</sub></b> (5%):TSPO1 (100 nm)) and the electroluminescent (EL) spectra of <b>f-Ir-(dbfmi)<sub>3</sub></b> and <b>m-Ir-(dbfmi)<sub>3</sub></b> .	S15
<b>Fig. S10</b>	TGA trace of <b>f-Ir-(dbfmi)<sub>3</sub></b> and <b>m-Ir-(dbfmi)<sub>3</sub></b> .	S16
<b>Table S5.</b>	Device structure and characteristics using <b>f-Ir-(dbfmi)<sub>3</sub></b> and <b>m-Ir-(dbfmi)<sub>3</sub></b> as dopants.	S17
<b>Fig. S11</b>	Device architecture and relative energy level of <b>f-Ir-(dbfmi)<sub>3</sub></b> and <b>m-Ir-(dbfmi)<sub>3</sub></b> .	S18
<b>Fig. S12</b>	Emission spectra and EL spectra of the device for <b>f-Ir-(dbfmi)<sub>3</sub></b> and <b>m-Ir-(dbfmi)<sub>3</sub></b> .	S19
		S20

## Synthetic details



**1-(dibenzo[*b,d*]furan-4-yl)-1*H*-imidazole (2).** 4-bromodibenzo[*b,d*]furan (2.5 g, 10 mmol) are dissolved in dimethylformamide (100 mL). Imidazole (0.8 g, 12 mmol), copper(I) iodide (0.35 g, 1.8 mmol), and K<sub>2</sub>CO<sub>3</sub> (1.88 g, 13 mmol) are added. The mixture is stirred for 48 h at 150 °C. After 24 h, another (0.08 g, 1.2 mmol) is added and after 44 h another (0.04 g, 0.6 mmol) imidazole is added. The solution is allowed to cool to room temperature and the insoluble parts are removed by filtration. The solvent is removed and the residue is dissolved in 100 mL CH<sub>2</sub>Cl<sub>2</sub>, and then washed with 15 mL NH<sub>3</sub> solution (25%) and 150 mL water. After separation of the phases, the organic solution is dried over MgSO<sub>4</sub> and filtered. The filtrates were dried under reduced pressure and used without further purification in the next reaction step.

**1-(dibenzo[*b,d*]furan-4-yl)-3-methyl-1*H*-imidazol-3-ium iodide (3).** 1-(dibenzo[*b,d*]furan-4-yl)-1*H*-imidazole (8 g, 34.1 mmol) of the previously described reaction step are dissolved in THF (100 mL). Methyl iodide (24 g, 0.17 mol) is then slowly added. The mixture is stirred for 65 h at room temperature. The precipitate is filtered, washed with THF (100 mL), and dried to isolate the beige coloured product. <sup>1</sup>H-NMR (DMSO-*d*<sub>6</sub>, 300 MHz, δ): 9.91 (s, 1H), 8.45 (t, *J* = 2.0 Hz, 1H), 8.41 (d, *J* = 7.2 Hz, 1H), 8.31 (d, *J* = 6.9 Hz, 1H), 8.08 (s, 1H), 7.91 (d, *J* = 7.5 Hz, 1H), 7.81 (d, *J* = 8.4 Hz, 1H), 7.70–7.63 (m, 2H), 7.53 (t, *J* = 6.9 Hz, 1H), 4.05 (s, 3H).

**General synthetic procedure of Iridium complexes.** Imidazolium salt (5 g, 13.3 mmol) and silver(I) oxide (1.54 g, 6.65 mmol) are dissolved in dioxane (280 mL) and stirred for 16 h at room temperature under an argon atmosphere. After the addition of di-μ-Chlorobis(1,5-cyclooctadiene)diiridium (2.95 g, 4.39 mmol), the mixture is heated and refluxed for 16 h. The reaction mixture was then cooled to room temperature and filtered. The filtrate was collected and two isomers were isolated by silica gel column chromatography using CH<sub>2</sub>Cl<sub>2</sub>/n-hexane = 1/1 (v/v) as an eluent. *R*<sub>f</sub> for **f-Ir-(dbfmi)<sub>3</sub>** = 0.35 and *R*<sub>f</sub> for **m-Ir-(dbfmi)<sub>3</sub>** = 0.50.

**f-Ir-(dbfmi)<sub>3</sub>:** <sup>1</sup>H-NMR (DMSO-*d*<sub>6</sub>, 300 MHz, δ): 8.28 (d, *J* = 1.5 Hz, 3H), 7.89 (d, *J* = 6.9 Hz, 3H), 7.68 (d, *J* = 8.4 Hz, 3H), 7.42 (t, *J* = 7.35 Hz, 3H), 7.34–7.21 (m, 9H), 6.50 (d, *J* = 7.8 Hz, 3H), 3.15 (s, 9H); ESI-MS calcd. for C<sub>48</sub>H<sub>36</sub>IrN<sub>6</sub>O<sub>3</sub> (934.2227); found 934.4571 [M]<sup>+</sup>. Anal. Calcd.: C, 61.72; H, 3.56; N, 9.00; O, 5.14. Found: C, 61.76; H, 3.62; N, 9.03; O, 5.17.

**m-Ir-(dbfmi)<sub>3</sub>:** <sup>1</sup>H-NMR (DMSO-*d*<sub>6</sub>, 300 MHz, δ): 8.39 (d, *J* = 2.1 Hz, 1H), 8.34 (d, *J* = 2.4 Hz, 1H), 8.22 (d, *J* = 1.5 Hz, 1H), 7.87 (t, *J* = 8.4 Hz, 1H), 7.67 (t, *J* = 7.35 Hz, 1H), 7.39–7.19 (m, 16H), 6.74 (d, *J* = 7.8 Hz, 1H), 6.67 (d, *J* = 7.5 Hz, 1H), 6.55 (d, *J* = 7.8 Hz, 1H), 3.13 (s, 3H), 3.05 (s, 3H), 2.99 (s, 3H); ESI-MS calcd. for C<sub>48</sub>H<sub>36</sub>IrN<sub>6</sub>O<sub>3</sub> (934.2227); found 934.2473 [M]<sup>+</sup>. Anal. Calcd.: C, 61.72; H, 3.56; N, 9.00; O, 5.14. Found: C, 61.74; H, 3.59; N, 9.03; O, 5.16.

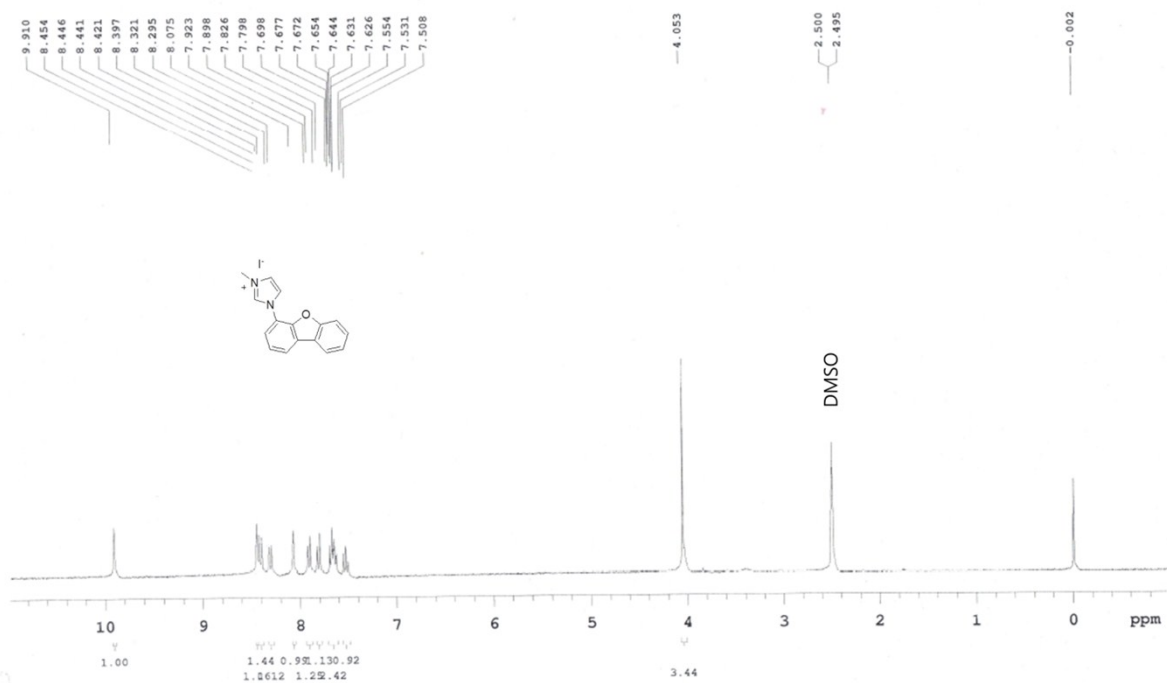


**Fig. S1**  $^1\text{H}$ -NMR spectra of 1-(dibenzo[*b,d*]furan-4-yl)-3-methyl-1*H*-imidazol-3-ium iodide.

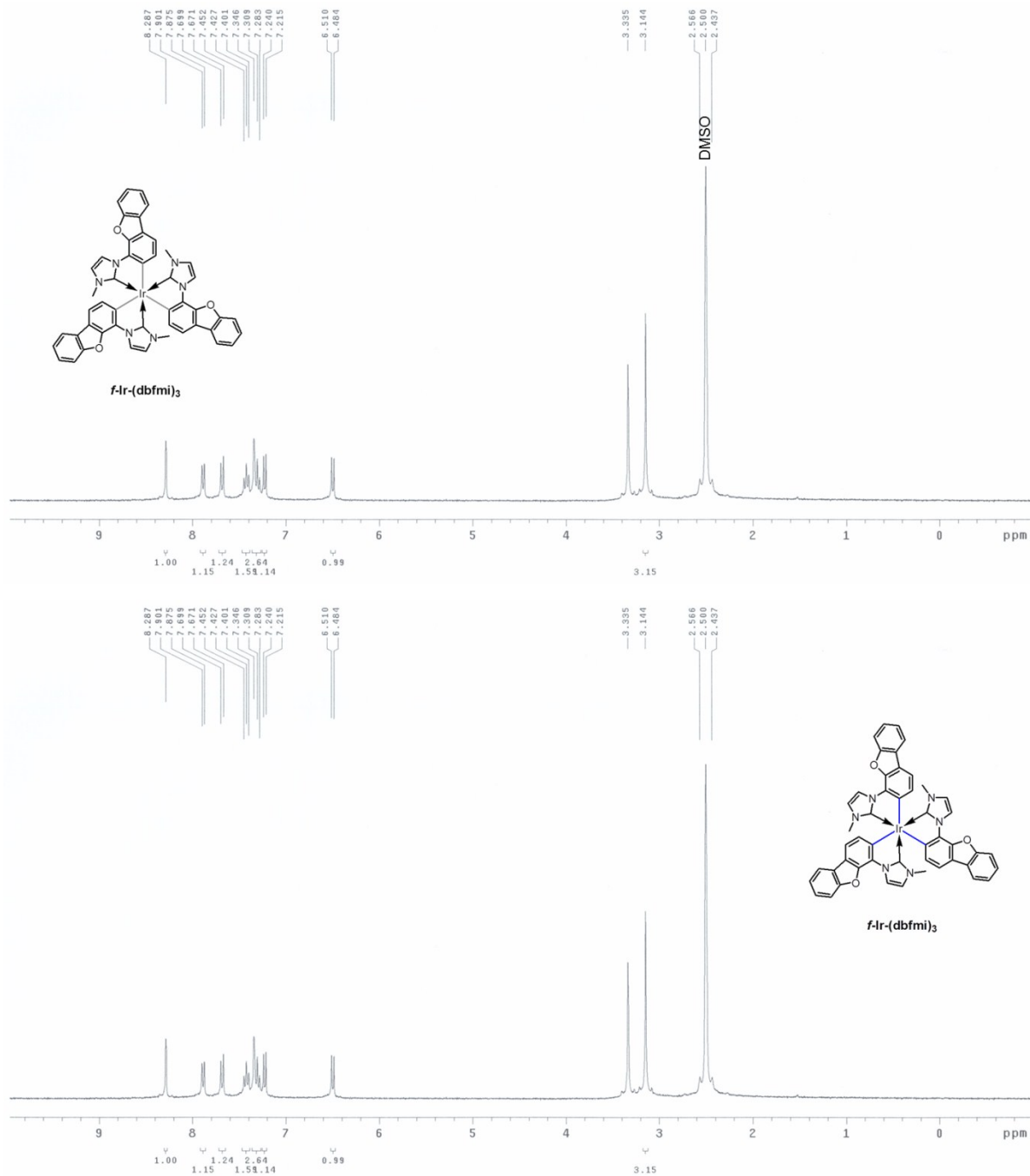


**Fig. S2** <sup>1</sup>H-NMR spectra of *f*-Ir-(dbfmi)<sub>3</sub> before (top) and after (down) vapor deposition.

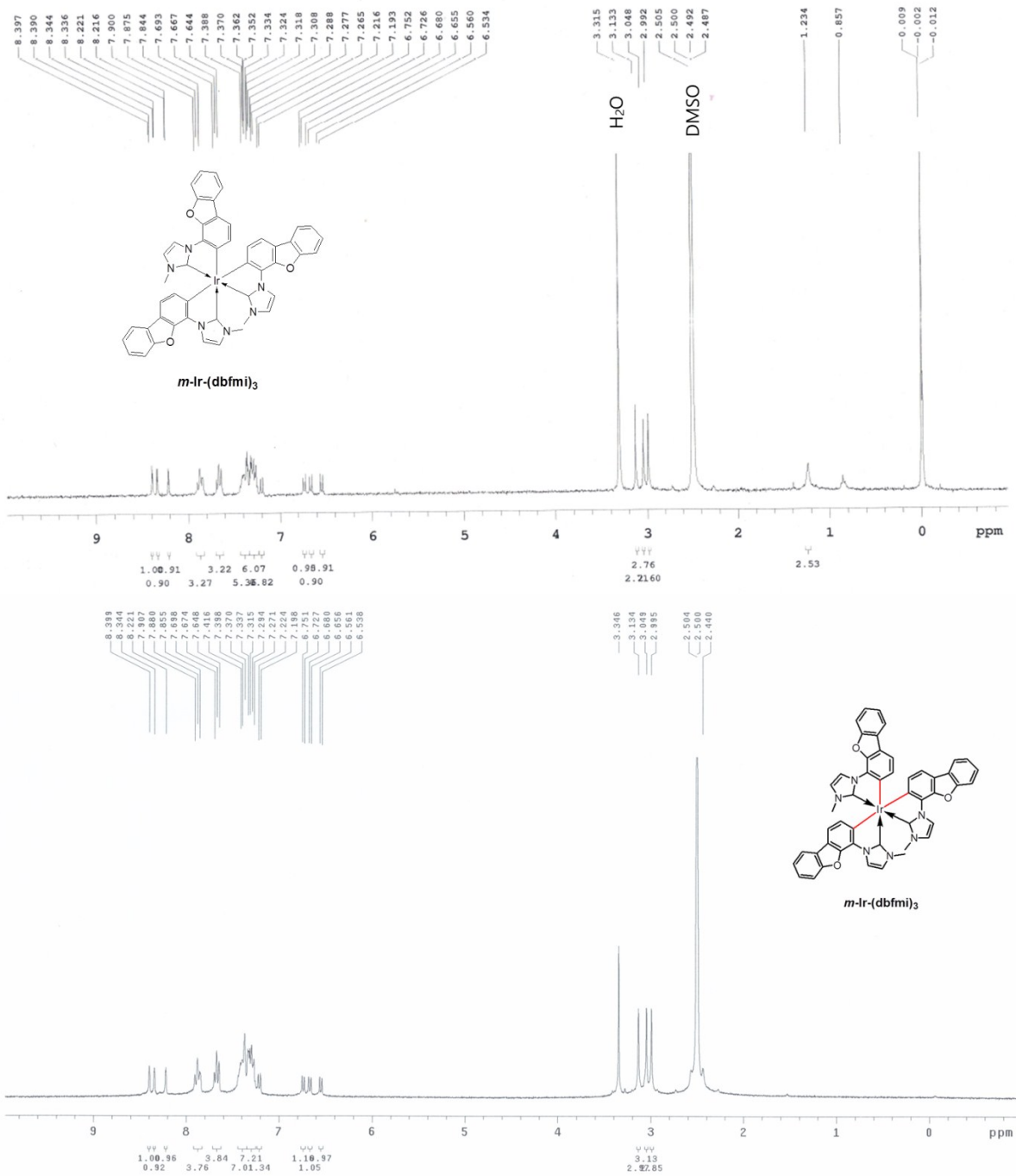


**Fig. S3**  $^1\text{H}$ -NMR spectra of *m*-Ir-(dbfmi)<sub>3</sub> before (top) and after (down) vapor deposition.

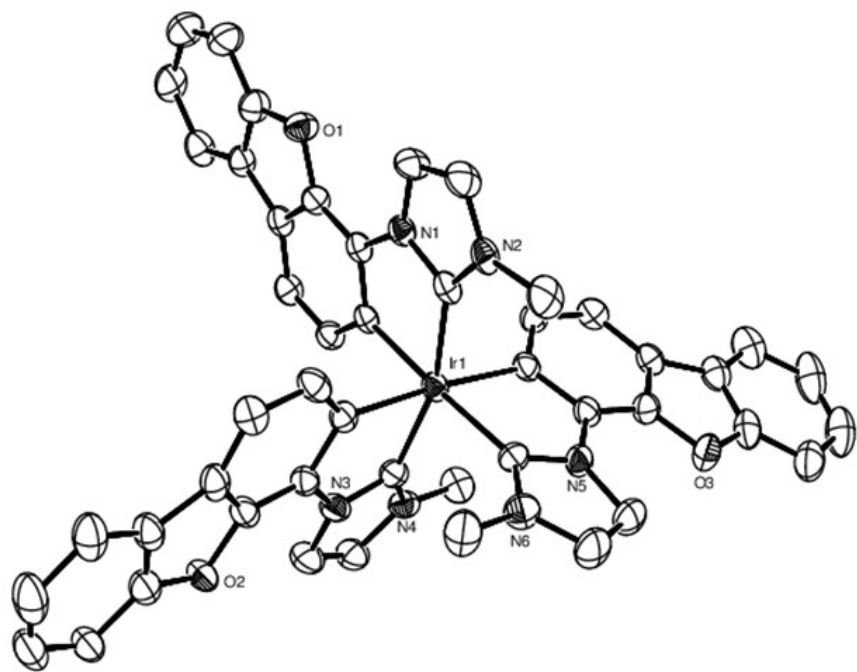


**Fig. S4** ORTEP drawing of compound *m*-Ir-(dbfmi)<sub>3</sub> with 30% probability for the thermal ellipsoids. Hydrogens were omitted for clarity.

**Table S1.** Crystal data and structure refinement for ***m*-Ir-(dbfmi)<sub>3</sub>**.

Identification code	<b><i>m</i>-Ir-(dbfmi)<sub>3</sub></b>	
Empirical formula	C <sub>48</sub> H <sub>33</sub> IrN <sub>6</sub> O <sub>3</sub>	
Formula weight	934.00	
Temperature	293(2) K	
Wavelength	0.71073 Å	
Crystal system, space group	<i>Triclinic</i> , <i>P</i> -1	
Unit cell dimensions	<i>a</i> = 13.381(6) Å	$\alpha$ = 105.045(9)°
	<i>b</i> = 13.771(7) Å	$\beta$ = 101.432(9)°
	<i>c</i> = 15.248(7) Å	$\gamma$ = 113.389(8)°
Volume	2342.2(19) Å <sup>3</sup>	
Z, Calculated density	2, 1.324 Mg/m <sup>3</sup>	
Absorption coefficient, $\mu$	2.894 mm <sup>-1</sup>	
<i>F</i> (000)	928	
Crystal size	0.3 × 0.18 × 0.1 mm	
$\theta$ range for data collection	1.47 to 28.28°	
Limiting indices	-17 ≤ <i>h</i> ≤ 17, -18 ≤ <i>k</i> ≤ 18, 20 ≤ <i>l</i> ≤ 20	
Reflections collected / unique	24175 / 9325 [ $R_{\text{int}} = 0.0459$ ]	
Completeness to $\theta = 28.40$	77.2 %	
Refinement method	Full-matrix least-squares on <i>F</i> <sup>2</sup>	
Data / restraints / parameters	9325 / 0 / 526	
Goodness-of-fit on <i>F</i> <sup>2</sup>	0.944	
Final <i>R</i> indices [ <i>I</i> >2σ( <i>I</i> )]	$R_1^a = 0.0360$ , $wR_2^b = 0.1032$	
<i>R</i> indices (all data)	$R_1 = 0.0559$ , $wR_2 = 0.10700$	
Largest diff. peak and hole	1.568 and -0.450 e.Å <sup>-3</sup>	

<sup>a</sup> $R_1 = \sum ||F_o| - |F_c||$  (based on reflections with  $F_o^2 > 2\sigma F^2$ ), <sup>b</sup> $wR_2 = [\sum [w(F_o^2 - F_c^2)^2] / \sum [w(F_o^2)^2]]^{1/2}$ ;  $w = 1/[\sigma^2(F_o^2) + (0.095P)^2]$ ;  $P = [\max(F_o^2, 0) + 2 F_c^2]/3$  (also with  $F_o^2 > 2\sigma F^2$ )

**Table S2.** Bond lengths [Å] for ***m*-Ir-(dbfmi)<sub>3</sub>**.

Ir(1)-C(15)	2.036(5)	C(5)-C(10)	1.370(9)
Ir(1)-C(31)	2.044(6)	C(5)-C(6)	1.394(9)
Ir(1)-C(47)	2.069(5)	C(6)-C(7)	1.399(1)
Ir(1)-C(1)	2.090(5)	C(7)-C(8)	1.360(1)
Ir(1)-C(17)	2.091(6)	C(8)-C(9)	1.360(1)
Ir(1)-C(33)	2.117(6)	C(9)-C(10)	1.380(8)
O(1)-C(11)	1.400(6)	C(11)-C(12)	1.381(8)
O(1)-C(10)	1.419(8)	C(13)-C(14)	1.335(9)
O(2)-C(26)	1.380(8)	C(17)-C(18)	1.399(8)
O(2)-C(27)	1.420(7)	C(17)-C(28)	1.422(8)
O(3)-C(42)	1.387(9)	C(18)-C(19)	1.389(9)
O(3)-C(43)	1.393(7)	C(19)-C(20)	1.402(9)
N(1)-C(15)	1.378(7)	C(20)-C(27)	1.399(9)
N(1)-C(13)	1.387(7)	C(20)-C(21)	1.441(9)
N(1)-C(12)	1.428(7)	C(21)-C(22)	1.397(1)
N(2)-C(15)	1.363(7)	C(21)-C(26)	1.416(1)
N(2)-C(14)	1.385(8)	C(22)-C(23)	1.410(1)
N(2)-C(16)	1.460(8)	C(23)-C(24)	1.359(1)
N(3)-C(31)	1.343(8)	C(24)-C(25)	1.369(1)
N(3)-C(29)	1.391(8)	C(25)-C(26)	1.392(1)
N(3)-C(28)	1.431(7)	C(27)-C(28)	1.362(8)
N(4)-C(31)	1.364(7)	C(29)-C(30)	1.384(1)
N(4)-C(30)	1.394(9)	C(33)-C(34)	1.409(7)
N(4)-C(32)	1.458(9)	C(33)-C(44)	1.417(8)
N(5)-C(47)	1.379(8)	C(34)-C(35)	1.385(9)
N(5)-C(44)	1.418(7)	C(35)-C(36)	1.421(9)
N(5)-C(45)	1.421(8)	C(36)-C(43)	1.417(8)
N(6)-C(47)	1.351(7)	C(36)-C(37)	1.451(9)
N(6)-C(46)	1.393(1)	C(37)-C(38)	1.393(1)
N(6)-C(48)	1.476(9)	C(37)-C(42)	1.397(1)
C(1)-C(12)	1.394(7)	C(38)-C(39)	1.425(1)
C(1)-C(2)	1.414(8)	C(39)-C(40)	1.363(1)
C(2)-C(3)	1.372(8)	C(40)-C(41)	1.436(1)
C(3)-C(4)	1.397(8)	C(41)-C(42)	1.391(1)
C(4)-C(11)	1.397(8)	C(43)-C(44)	1.374(9)
C(4)-C(5)	1.441(8)	C(45)-C(46)	1.366(1)

**Table S3.** Angles [°] for ***m*-Ir-(dbfmi)<sub>3</sub>**.

C(15)-Ir(1)-C(31)	164.1(2)	N(2)-C(15)-N(1)	103.9(5)
C(15)-Ir(1)-C(47)	104.3(2)	N(2)-C(15)-Ir(1)	139.7(4)
C(31)-Ir(1)-C(47)	89.0(2)	N(1)-C(15)-Ir(1)	116.1(4)
C(15)-Ir(1)-C(1)	78.2(2)	C(18)-C(17)-C(28)	115.3(5)
C(31)-Ir(1)-C(1)	89.6(2)	C(18)-C(17)-Ir(1)	130.8(4)
C(47)-Ir(1)-C(1)	173.1(2)	C(28)-C(17)-Ir(1)	113.9(4)
C(15)-Ir(1)-C(17)	91.0(2)	C(19)-C(18)-C(17)	125.0(5)
C(31)-Ir(1)-C(17)	78.5(2)	C(18)-C(19)-C(20)	117.7(6)
C(47)-Ir(1)-C(17)	97.2(2)	C(27)-C(20)-C(19)	118.6(6)
C(1)-Ir(1)-C(17)	89.1(2)	C(27)-C(20)-C(21)	106.2(6)
C(15)-Ir(1)-C(33)	92.2(2)	C(19)-C(20)-C(21)	135.2(6)
C(31)-Ir(1)-C(33)	99.2(2)	C(22)-C(21)-C(26)	117.6(7)
C(47)-Ir(1)-C(33)	78.5(2)	C(22)-C(21)-C(20)	136.7(7)
C(1)-Ir(1)-C(33)	95.1(2)	C(26)-C(21)-C(20)	105.7(6)
C(17)-Ir(1)-C(33)	175.18(2)	C(21)-C(22)-C(23)	118.1(8)
C(11)-O(1)-C(10)	104.4(4)	C(24)-C(23)-C(22)	122.6(8)
C(26)-O(2)-C(27)	104.5(5)	C(23)-C(24)-C(25)	121.0(7)
C(42)-O(3)-C(43)	106.2(5)	C(24)-C(25)-C(26)	117.8(8)
C(15)-N(1)-C(13)	111.1(5)	O(2)-C(26)-C(25)	124.8(7)
C(15)-N(1)-C(12)	116.4(4)	O(2)-C(26)-C(21)	112.2(6)
C(13)-N(1)-C(12)	132.3(5)	C(25)-C(26)-C(21)	123.0(7)
C(15)-N(2)-C(14)	110.3(5)	C(28)-C(27)-C(20)	122.6(5)
C(15)-N(2)-C(16)	123.8(5)	C(28)-C(27)-O(2)	125.9(6)
C(14)-N(2)-C(16)	125.8(5)	C(20)-C(27)-O(2)	111.5(5)
C(31)-N(3)-C(29)	112.7(5)	C(27)-C(28)-C(17)	120.8(5)
C(31)-N(3)-C(28)	117.1(4)	C(27)-C(28)-N(3)	125.6(5)
C(29)-N(3)-C(28)	129.7(6)	C(17)-C(28)-N(3)	113.6(5)
C(31)-N(4)-C(30)	110.8(6)	C(30)-C(29)-N(3)	105.0(6)
C(31)-N(4)-C(32)	126.0(5)	C(29)-C(30)-N(4)	106.8(6)
C(30)-N(4)-C(32)	123.1(5)	N(3)-C(31)-N(4)	104.8(5)
C(47)-N(5)-C(44)	117.8(5)	N(3)-C(31)-Ir(1)	116.8(4)
C(47)-N(5)-C(45)	112.7(5)	N(4)-C(31)-Ir(1)	138.1(4)
C(44)-N(5)-C(45)	129.5(6)	C(34)-C(33)-C(44)	116.7(5)
C(47)-N(6)-C(46)	110.9(6)	C(34)-C(33)-Ir(1)	129.5(4)
C(47)-N(6)-C(48)	125.6(6)	C(44)-C(33)-Ir(1)	113.8(4)
C(46)-N(6)-C(48)	123.5(5)	C(35)-C(34)-C(33)	123.3(6)
C(12)-C(1)-C(2)	116.6(5)	C(34)-C(35)-C(36)	119.4(5)
C(12)-C(1)-Ir(1)	115.2(4)	C(43)-C(36)-C(35)	117.5(6)

C(2)-C(1)-Ir(1)	128.2(4)	C(43)-C(36)-C(37)	105.8(5)
C(3)-C(2)-C(1)	123.9(5)	C(35)-C(36)-C(37)	136.6(6)
C(2)-C(3)-C(4)	118.2(5)	C(38)-C(37)-C(42)	118.3(7)
C(11)-C(4)-C(3)	119.1(5)	C(38)-C(37)-C(36)	135.6(7)
C(11)-C(4)-C(5)	106.3(5)	C(42)-C(37)-C(36)	106.0(6)
C(3)-C(4)-C(5)	134.5(5)	C(37)-C(38)-C(39)	118.8(8)
C(10)-C(5)-C(6)	118.2(5)	C(40)-C(39)-C(38)	121.9(9)
C(10)-C(5)-C(4)	106.7(5)	C(39)-C(40)-C(41)	120.4(8)
C(6)-C(5)-C(4)	135.1(6)	C(42)-C(41)-C(40)	116.3(8)
C(5)-C(6)-C(7)	119.0(6)	O(3)-C(42)-C(41)	124.1(7)
C(8)-C(7)-C(6)	120.2(7)	O(3)-C(42)-C(37)	111.5(6)
C(9)-C(8)-C(7)	121.7(7)	C(41)-C(42)-C(37)	124.3(7)
C(8)-C(9)-C(10)	117.8(7)	C(44)-C(43)-O(3)	127.4(5)
C(5)-C(10)-C(9)	123.0(6)	C(44)-C(43)-C(36)	122.2(6)
C(5)-C(10)-O(1)	111.6(5)	O(3)-C(43)-C(36)	110.4(5)
C(9)-C(10)-O(1)	125.4(6)	C(43)-C(44)-C(33)	120.8(5)
C(12)-C(11)-C(4)	121.8(5)	C(43)-C(44)-N(5)	124.8(5)
C(12)-C(11)-O(1)	127.1(5)	C(33)-C(44)-N(5)	114.4(5)
C(4)-C(11)-O(1)	111.1(5)	C(46)-C(45)-N(5)	103.0(7)
C(11)-C(12)-C(1)	120.3(5)	C(45)-C(46)-N(6)	109.4(6)
C(11)-C(12)-N(1)	126.0(5)	N(6)-C(47)-N(5)	103.9(5)
C(1)-C(12)-N(1)	113.7(4)	N(6)-C(47)-Ir(1)	140.7(5)
C(14)-C(13)-N(1)	106.1(5)	N(5)-C(47)-Ir(1)	115.0(4)
C(13)-C(14)-N(2)	108.4(5)		

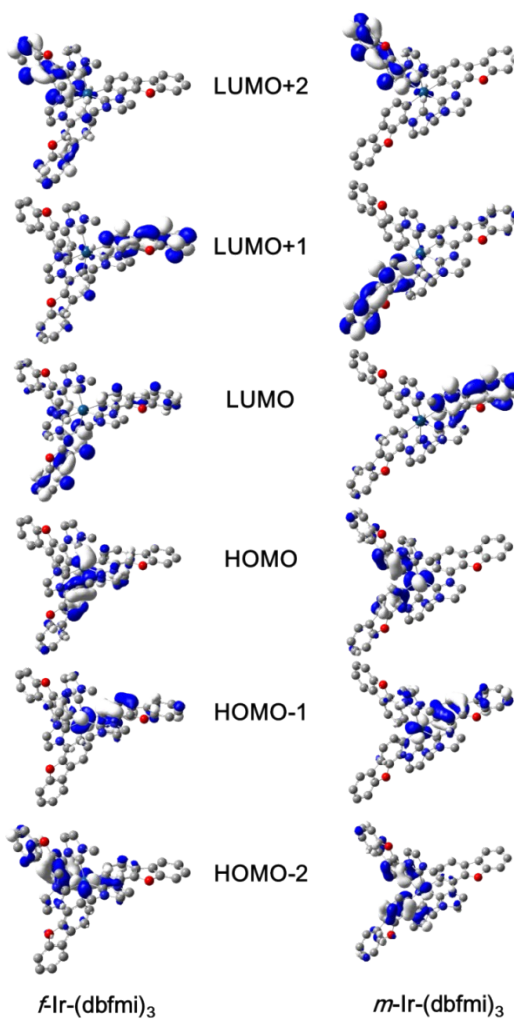


**Fig. S5** Contour plots of selected orbitals calculated for *f*-Ir-(dbfmi)<sub>3</sub> (left) and *m*-Ir-(dbfmi)<sub>3</sub> (right) in the singlet ground state geometry.

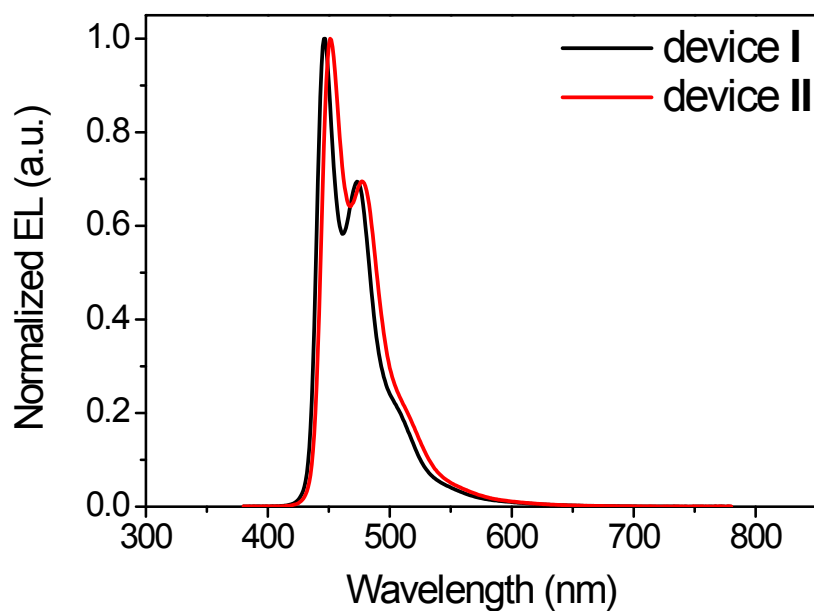


**Fig. S6** The electroluminescent (EL) spectra of device **I** and **II**.

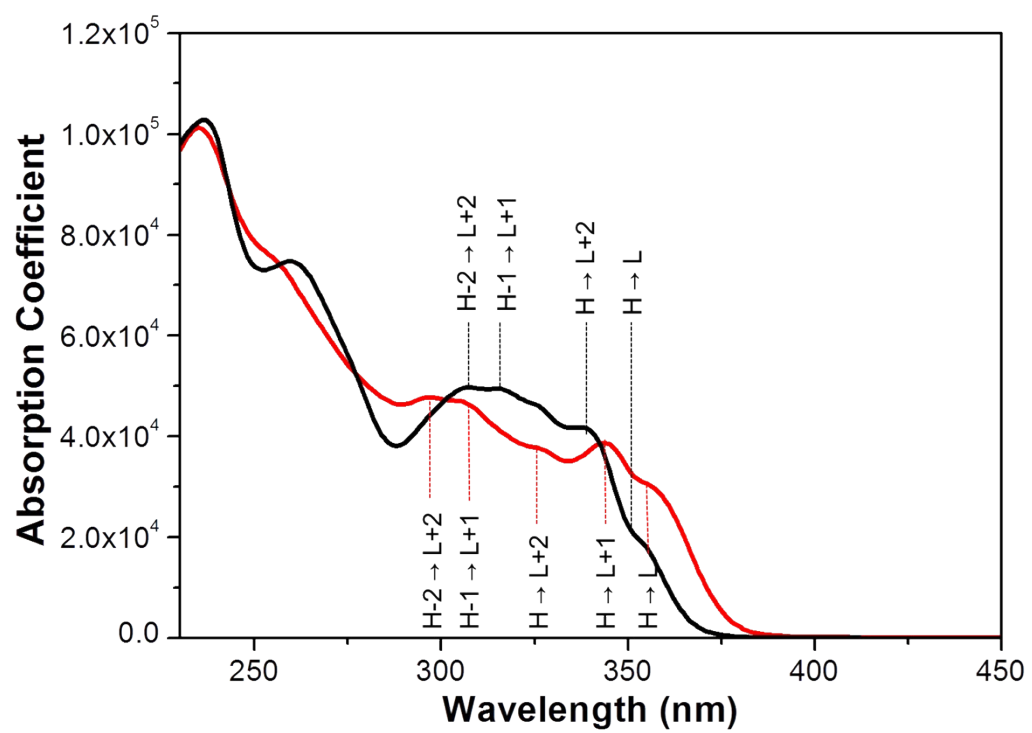


**Fig. S7** Experimental absorption spectra and calculated singlet transition for *f*-Ir-(dbfmi)<sub>3</sub> (black) and *m*-Ir-(dbfmi)<sub>3</sub> (red).

**Table S4.** Energy levels of the lower lying transitions of complex **f-Ir-(dbfmi)<sub>3</sub>** and **m-Ir-(dbfmi)<sub>3</sub>** calculated from the TD-DFT approach.

	State	Assgnt	$\lambda$ (nm)	$(f)$
<b>f-Ir-(dbfmi)<sub>3</sub></b>	S	HOMO→LUMO (86%)	349.7	0.1242
	S	HOMO→LUMO+2 (85%)	340.0	0.0986
	S	HOMO→LUMO+1 (78%)	333.3	0.0466
	S	HOMO-1→LUMO+1 (76%)	318.1	0.2925
	S	HOMO-2→LUMO+2 (43%); HOMO→LUMO+3 (24%)	305.0	0.1348
	T	HOMO→LUMO (18%); HOMO→LUMO+2 (48%); HOMO→LUMO+3 (-10%)	354.1	-
<b>m-Ir-(dbfmi)<sub>3</sub></b>	S	HOMO→LUMO (93%)	347.7	0.0588
	S	HOMO→LUMO+1 (89%)	340.1	0.0996
	S	HOMO→LUMO+2 (85%)	330.9	0.1119
	S	HOMO-1→LUMO+1 (92%)	313.9	0.1399
	S	HOMO-2→LUMO+2 (13%), HOMO→LUMO+5 (41%)	294.1	0.3341
	T	HOMO→LUMO (54%)	348.2	-

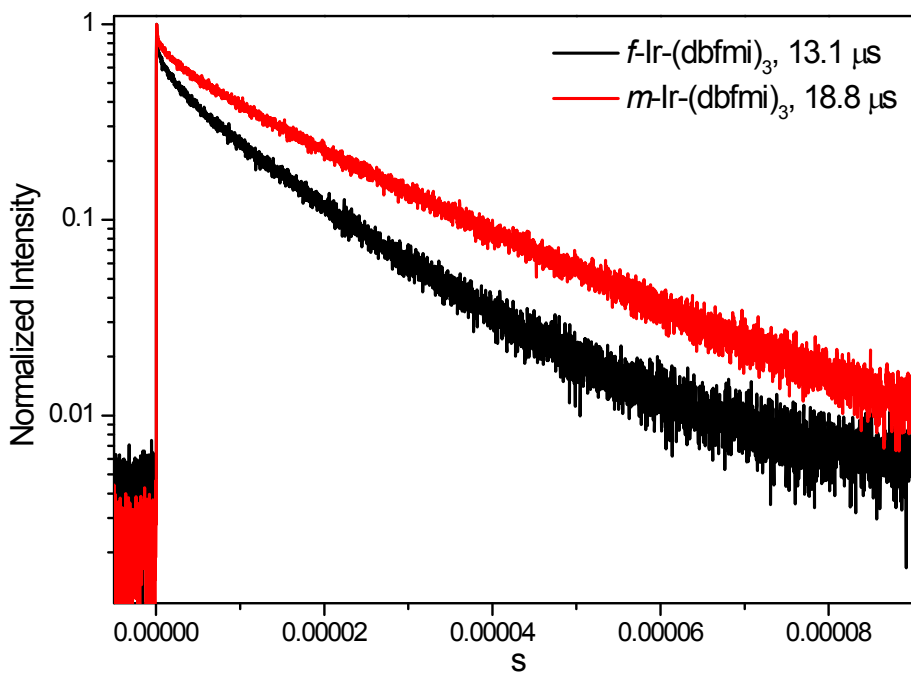


**Fig. S8** Emission decay profiles for  $f\text{-Ir-(dbfmi)}_3$  and  $m\text{-Ir-(dbfmi)}_3$  in doped films of ( $f\text{-Ir-(dbfmi)}_3$  or  $m\text{-Ir-(dbfmi)}_3$ ) (5%):TSPO1 (100 nm)).

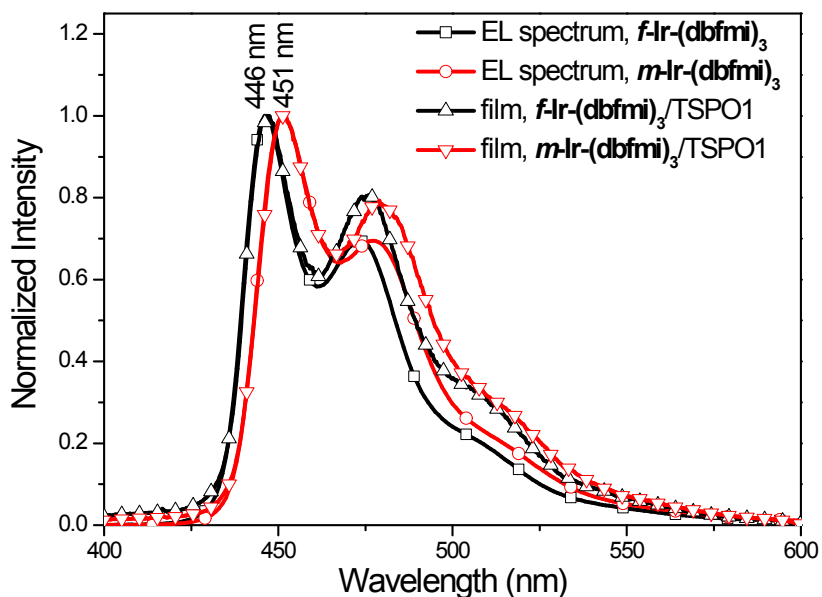


**Fig. S9** Emission spectra of *f*-Ir-(dbfmi)<sub>3</sub> and *m*-Ir-(dbfmi)<sub>3</sub> in doped films (*f*-Ir-(dbfmi)<sub>3</sub> or *m*-Ir-(dbfmi)<sub>3</sub> (5%):TSPO1 (100 nm)) and the electroluminescent (EL) spectra of *f*-Ir-(dbfmi)<sub>3</sub> and *m*-Ir-(dbfmi)<sub>3</sub>.

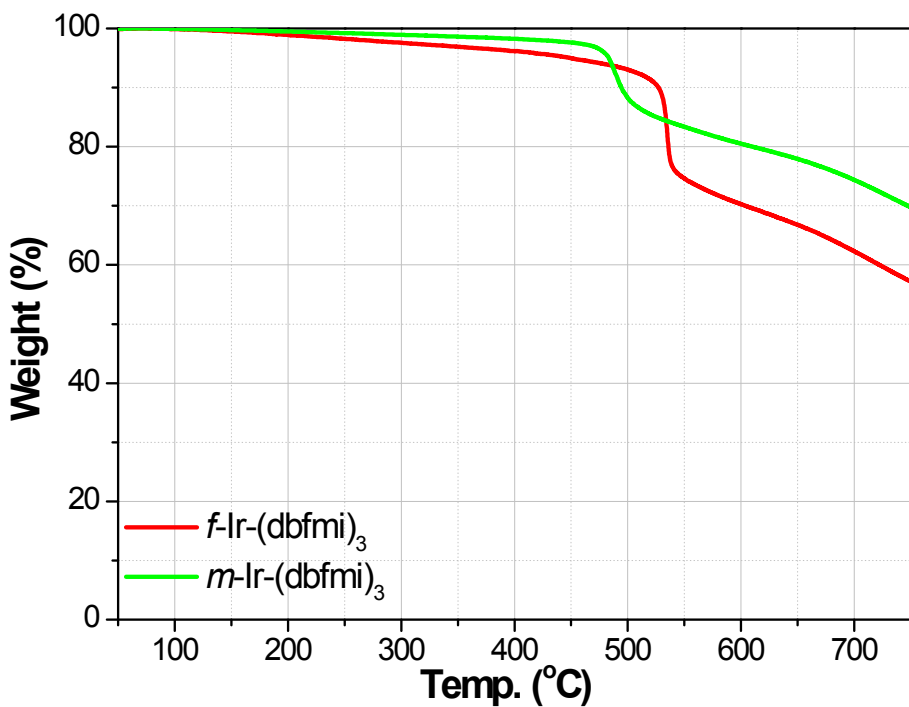


Fig. S10 TGA traces of *f*-Ir-(dbfmi)<sub>3</sub> and *m*-Ir-(dbfmi)<sub>3</sub>.

**Table S5.** Device structure and characteristics using **f-Ir-(dbfmi)<sub>3</sub>** and **m-Ir-(dbfmi)<sub>3</sub>** as dopants.

	Current efficiency (cd/A)			Power efficiency (lm/W)			Turn-on voltage (V)	CIE (x, y)	EQE (%)		
	100 cd m <sup>-2</sup>	1000 cd m <sup>-2</sup>	Max	100 cd m <sup>-2</sup>	1000 cd m <sup>-2</sup>	Max			100 cd m <sup>-2</sup>	1000 cd m <sup>-2</sup>	Max
Reference	20.5	9.4	28.6	19.6	6.3	35.9	2.56	(0.15,0.19)	13.3	6.2	18.6
device I	14.5	4.1	18.6	12.3	1.8	19.4	2.6	(0.14, 0.11)	14.4	4.1	18.5
device II	16.3	3.9	18.8	13.8	1.5	23.6	2.5	(0.14, 0.14)	14.4	3.4	18.2

Reference: *Adv. Mater.*, 2010, **22**, 5003

Device structure: [ITO (130 nm)/TAPC (40 nm)/**m-Ir-(dbfmi)<sub>3</sub>** (10%):PO9 (20 nm)/PO9 (10 nm)/B3PyPB (30 nm)/Liq/Al (100 nm)]

Device I: [ITO (150 nm)/HAT-CN (10 nm)/TAPC (55 nm)/**f-Ir-(dbfmi)<sub>3</sub>** (10%):TSPO1 (20 nm)/TSPO1 (5 nm)/TmPyPB (30 nm)/Liq/Al (150 nm)]

Device II: [ITO (150 nm)/HAT-CN (10 nm)/TAPC (55 nm)/**m-Ir-(dbfmi)<sub>3</sub>** (10%):TSPO1 (20 nm)/TSPO1 (5 nm)/TmPyPB (30 nm)/Liq/Al (150 nm)]

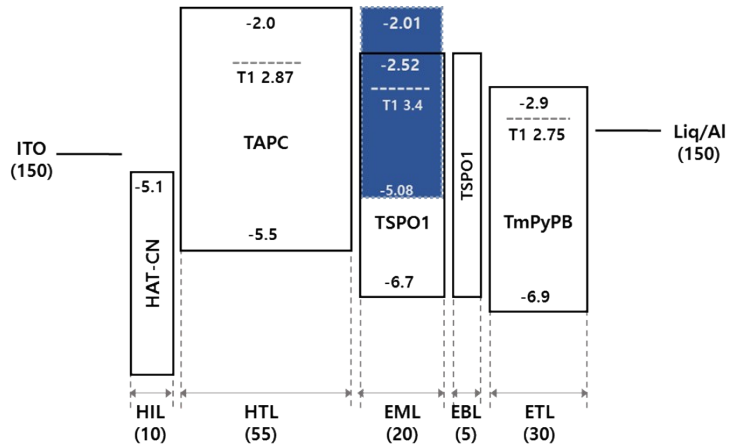


**Fig. S11** Device architecture and relative energy level of *f*-Ir-(dbfmi)<sub>3</sub> and *m*-Ir-(dbfmi)<sub>3</sub>.

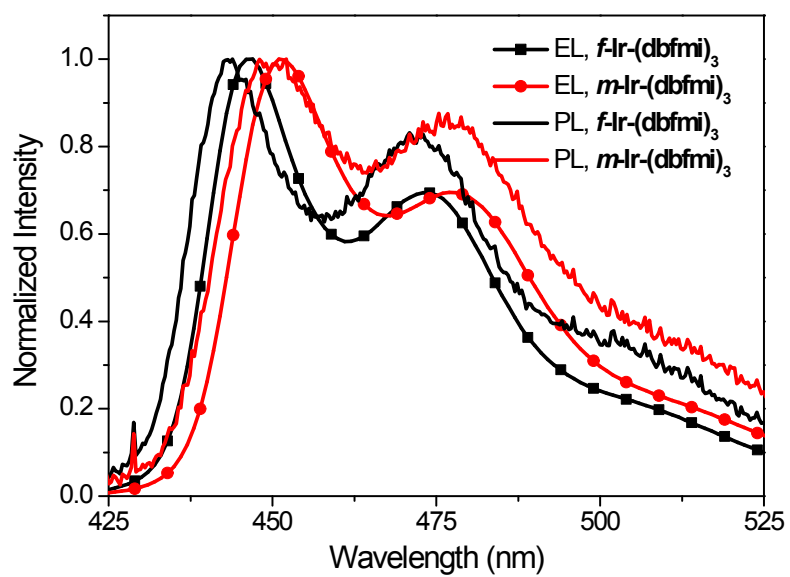


**Fig. S12** Emission spectra and EL spectra of the device for *f*-Ir-(dbfmi)<sub>3</sub> and *m*-Ir-(dbfmi)<sub>3</sub>.